

One- versus two-pole $\bar{K}N - \pi\Sigma$ potential: K^-d scattering length

N.V. Shevchenko¹

¹*Nuclear Physics Institute, 25068 Řež, Czech Republic*

(Dated: March 6, 2018)

Abstract

We investigated the dependence of the K^-d scattering length on models of $\bar{K}N$ interaction with one or two poles for $\Lambda(1405)$ resonance. The $\bar{K}NN - \pi\Sigma N$ system is described by coupled-channel Faddeev equations in AGS form. Our new two-body $\bar{K}N - \pi\Sigma$ potentials reproduce all existing experimental data on K^-p scattering and kaonic hydrogen atom characteristics. New models of $\Sigma N - \Lambda N$ interaction were also constructed. Comparison with several approximations, usually used for scattering length calculations, was performed.

PACS numbers: 13.75.Jz, 11.80.Gw

I. INTRODUCTION

Investigation of K^-d system can shed more light on the $\bar{K}N$ interaction, necessary for study of antikaonic nuclear clusters, which attracted large interest recently [1]. The interaction is not very well known, in particular, there are debates about the nature of the $\Lambda(1405)$ resonance. The question is whether it is a single resonance in $\pi\Sigma$ and a quasi-bound state in $\bar{K}N$ channel or the bump, which is usually understood as $\Lambda(1405)$ resonance, is an effect of two poles. The advantage of the K^-d system is the possibility of proper description of its dynamics using Faddeev equations [2].

Recently we constructed coupled-channel $\bar{K}N - \pi\Sigma$ potentials in one- and two-pole form [3], which reproduce all existing experimental data on K^-p scattering and K^-p atom characteristics equally well, therefore it is not possible to give preference to any of the versions. A possible way to clarify the question concerning the nature of the $\Lambda(1405)$ resonance is to perform few- or many-body calculations using one- and two-pole $\bar{K}N - \pi\Sigma$ potentials as an input. Having in mind SIDDHARTA experiment [4], measuring characteristics of kaonic deuterium atom, we calculated K^-d scattering length a_{K^-d} and investigated the dependence of the results on the models of $\bar{K}N$ interaction with newly obtained parameters. The scattering length gives possibility to calculate kaonic deuterium level shift and width. Comparison of the theoretical results with experimental ones could allow to choose between the two $\bar{K}N - \pi\Sigma$ interaction versions.

Dependence of a_{K^-d} on other two-body interactions, necessary for the description of the $\bar{K}NN - \pi\Sigma N$ system, was also investigated: we used several models of NN (with and without short range repulsion) and $\Sigma N(-\Lambda N)$ interactions. In addition to the full coupled-channel calculation we performed checks of commonly used approximations for K^-d scattering. In particular, we solved one-channel Faddeev equations using exact optical and simple complex $\bar{K}N$ potentials approximating the $\bar{K}N - \pi\Sigma$ models of interaction. We also checked the “Fixed center approximation to Faddeev equations” formula.

The formalism used for the coupled-channel K^-d scattering length calculation is described in the next section. Section III is devoted to the two-body input: the description of the one- and two-pole $\bar{K}N - \pi\Sigma$ potentials with newly obtained parameters in the first subsection is supplemented with additional arguments for equivalence of the two versions. The following subsections of Section III are devoted to NN and $\Sigma N - \Lambda N$ potentials. Section IV contains

information about approximate methods, usually used in K^-d scattering length calculations. The full and approximate results are shown and discussed in Section V, while Section VI concludes the paper.

II. COUPLED-CHANNEL AGS EQUATIONS FOR $\bar{K}NN - \pi\Sigma N$ SYSTEM

As in [6, 7] we directly include $\pi\Sigma N$ channel into original three-body Faddeev equations in the Alt-Grassberger-Sandhas (AGS) form [5], which leads to the coupled-channel equations:

$$U_{ij}^{\alpha\beta} = \delta_{\alpha\beta} (1 - \delta_{ij}) (G_0^\alpha)^{-1} + \sum_{k,\gamma=1}^3 (1 - \delta_{ik}) T_k^{\alpha\gamma} G_0^\gamma U_{kj}^{\gamma\beta}, \quad (1)$$

where ‘‘particle channel’’ indices $\alpha, \beta = 1, 2, 3$ are introduced in addition to the usual Faddeev partition indices $i, j, k = 1, 2, 3$, see Table I of [7]. The equations define unknown operators $U_{ij}^{\alpha\beta}$, describing the elastic and re-arrangement processes $j^\beta + (k^\beta i^\beta) \rightarrow i^\alpha + (j^\alpha k^\alpha)$. The free Green’s function is diagonal in channel indices: $G_0^{\alpha\beta} = \delta_{\alpha\beta} G_0^\alpha$. The inputs for the system of equations (1) are two-body T -matrices, embedded into three-body space: $T_i^{\alpha\beta}$ describes the interaction between the particles j and k ($i \neq j \neq k$) in channels α, β . Like in [7], here we have T_i^{NN} , $T_i^{\pi N}$ and $T_i^{\Sigma N}$, which are usual one-channel two-body T -matrices in three-body space, describing NN , πN , and ΣN interactions, respectively. The T_i^{KK} , $T_i^{\pi\pi}$, $T_i^{\pi K}$, and $T_i^{K\pi}$ are elements of the coupled-channel T -matrix for the $\bar{K}N - \pi\Sigma$ system.

In contrast to the calculation of the quasi-bound K^-pp state [7], where one-term isospin (I) dependent separable potentials were used, now we write AGS equations for N -term isospin dependent separable potentials

$$V_{i,I}^{\alpha\beta} = \sum_{m=1}^{N_i^\alpha} \lambda_{i(m),I}^{\alpha\beta} |g_{i(m),I}^\alpha\rangle \langle g_{i(m),I}^\beta|, \quad (2)$$

which lead to separable T -matrices

$$T_{i,I}^{\alpha\beta} = \sum_{m,n=1}^{N_i^\alpha} |g_{i(m),I}^\alpha\rangle \tau_{i(mn),I}^{\alpha\beta} \langle g_{i(n),I}^\beta|. \quad (3)$$

Here N_i^α is a number of terms of the separable potential, λ is a strength constant, while g is a form-factor. Bound state wave function of the two-body subsystem, described by such a potential, has the form

$$|\psi_{i,I}^\alpha\rangle = \sum_{m=1}^{N_i^\alpha} C_{i(m),I}^\alpha G_0^\alpha(z_{bnd}) |g_{i(m),I}^\alpha\rangle, \quad (4)$$

where the coefficients $C_{i(m),I}^\alpha$ are constants and z_{bnd} is a binding energy. We used two slightly different versions of a two-term nucleon-nucleon separable potential ($N_i^\alpha = 2$) in the a_{K-d} calculations. All other models of interactions, one more V^{NN} among them, are one-term potentials with $N_i^\alpha = 1$.

The amplitude $f_{ij,I_i I_j}^{\alpha\beta}$ of the $\bar{K}(NN) \rightarrow \bar{K}(NN)$ reaction with NN in isospin-zero state in the initial and final states is defined by the following matrix element:

$$f_{11,00}^{11}(\vec{p}_1^1, \vec{p}'_1^1; z_{tot}) = -(2\pi)^2 \mu_1^1 \langle \vec{p}_1^1; \psi_{1,0}^1 | U_{11,00}^{11}(z_{tot}) | \psi_{1,0}^1; \vec{p}'_1^1 \rangle, \quad (5)$$

where μ_i^α is the three-body reduced mass defined by

$$\mu_i^\alpha = \frac{m_i^\alpha(m_j^\alpha + m_k^\alpha)}{m_i^\alpha + m_j^\alpha + m_k^\alpha}, \quad i \neq j \neq k, \quad (6)$$

\vec{p}_1^1 and \vec{p}'_1^1 are initial and final relative momenta of antikaon with respect to the NN pair, correspondingly, while z_{tot} is the total energy of the three-body system. Deuteron wave function $\psi_{1,0}^1$ in Eq.(5) is defined by Eq.(4), the transition operator $U_{ij,I_i I_j}^{\alpha\beta}$ has two additional isospin indices compared to Eq.(1). The scattering length is the amplitude at zero kinetic energy z_{kin}^α :

$$a_{K-d} = f_{11,00}^{11}(\vec{p}_1^1 \rightarrow 0, \vec{p}'_1^1 \rightarrow 0; z_{tot} \rightarrow z_{th}^1) \quad (7)$$

with $z_{th}^\alpha = \sum_{i=1}^3 m_i^\alpha$ being the $\bar{K}NN$ ($\alpha = 1$) or $\pi\Sigma N$ ($\alpha = 2$) threshold energy (the total energy is defined by $z_{tot} = z_{kin}^\alpha + z_{th}^\alpha$).

Taking into account forms of T -matrices (3) and wave functions (4), introducing new operators

$$X_{i(m)j,I_i I_j}^{\alpha\beta} \equiv \langle g_{i(m),I_i}^\alpha | G_0^\alpha U_{ij,I_i I_j}^{\alpha\beta} | \psi_{j,I_j}^\beta \rangle, \quad (8)$$

$$Z_{i(m)j(n),I_i I_j}^{\alpha\beta} \equiv \delta_{\alpha\beta} Z_{i(m)j(n),I_i I_j}^\alpha = \delta_{\alpha\beta} (1 - \delta_{ij}) \langle g_{i(m),I_i}^\alpha | G_0^\alpha | g_{j(n),I_j}^\alpha \rangle, \quad (9)$$

and substituting them into the system (1), we can write a system of equations for the new unknown operators $X_{ij,I_i I_j}^{\alpha\beta}$:

$$\begin{aligned} X_{i(l)j,I_i I_j}^{\alpha\beta} &= \delta_{\alpha\beta} \sum_{m=1}^{N_j^\alpha} C_{j(m)}^\alpha Z_{i(l)j(m),I_i I_j}^\alpha + \\ &+ \sum_{k,\gamma=1}^3 \sum_{m,n=1}^{N_k^\alpha} \sum_{I_k} Z_{i(l)k(m),I_i I_k}^\alpha \tau_{k(mn),I_k}^{\alpha\gamma} X_{k(n)j,I_k I_j}^{\gamma\beta}. \end{aligned} \quad (10)$$

The number of equations in the system (10) is defined by the number of all form-factors g . Therefore, the system (10) with a two-term NN and one-term other potentials consists of 20 equations.

Two identical nucleons, entering the first ($\bar{K}NN$) channel, require antisymmetrization of the system of equations. Orbital momentum of all two-body interactions was set to zero. The main $\bar{K}N - \pi\Sigma$ potential was constructed with orbital momentum $l = 0$ since the interaction is dominated by the s -wave $\Lambda(1405)$ resonance. The interaction of π -meson with the nucleon is mainly in p -wave, however, as it was shown in [38], the addition of “small two-body interactions”, πN among them, changes the resulting a_{K-d} very slightly (of the order of 1% or even less, see Table XIII of the paper). On the other hand, s -wave πN interaction is even weaker, therefore, we omitted πN interaction in our equations. Information about ΣN interaction is very poor, and there is no reason to assume significant effect of higher partial waves. Finally, NN interaction was also taken in $l = 0$ state only since we do not see physical reasons for sufficient effect of higher partial waves in the present calculation.

Antisymmetric s -wave deuteron wave function has zero isospin and spin equal to one. Due to this K^-d system, in contrast to K^-pp [6, 7], has total three-body spin (and total momentum) equal to one, while both $\bar{K}NN$ systems have total isospin $I = \frac{1}{2}$. Therefore, in the K^-d case antisymmetrization leads to the following new operators:

$$\begin{aligned} X_{1(m),0}^{1,asm} &= X_{1(m),0}^1, & X_{2,I}^{1,asm} &= X_{2,I}^1 - X_{3,I}^1, \\ X_{1,\frac{1}{2}}^{2,asm} &= X_{1,\frac{1}{2}}^2 + X_{1,\frac{1}{2}}^3, & X_{1,\frac{3}{2}}^{2,asm} &= X_{1,\frac{3}{2}}^2 - X_{1,\frac{3}{2}}^3, \\ X_{2,I}^{2,asm} &= X_{2,I}^2 - X_{3,I}^3, & X_{3,I}^{2,asm} &= X_{3,I}^2 - X_{2,I}^3. \end{aligned} \quad (11)$$

It is necessary to note, that the \bar{K}^0nn state drops out from the system of equations (10) after the antisymmetrization because the two neutrons are in isospin one state. Therefore the \bar{K}^0nn channel has another value of the three-body spin ($S = 0$) than K^-d ($S = 1$) or the neutrons does not satisfy Pauli principle.

Finally, K^-d scattering length can be found from

$$a_{K-d} = -(2\pi)^2 \mu_1^1 \sum_{m=1}^2 C_{1(m),0}^1 X_{1(m),0}^{1,asm}(0, 0; z_{th}^1). \quad (12)$$

The operator system (10) written in momentum space turns into a system of integral equations. In order to solve the inhomogeneous system we transformed the integral equations into algebraic ones. It is known (see. e.g. [8]), that integral Faddeev equations have moving logarithmic singularities in the kernels when scattering above a three-body threshold

($z_{kin} > 0$) is described. “Usual” (one-channel) scattering length calculations are free of the singularities. For the $\bar{K}NN - \pi\Sigma N$ system, however, where $z_{th}^2 < z_{th}^1$, the permanently opened $\pi\Sigma N$ channel causes appearance of logarithmic singularities in K^{-d} scattering length calculations. In the numerical procedure we handle them using the method suggested in [9]. The main idea of the method consists in interpolating the unknown solutions (in the interval containing the singular points) by certain polynomials and subsequent analytic integration of the singular part of the kernels.

III. TWO-BODY INPUT

The separable $\bar{K}N - \pi\Sigma$, NN , and ΣN potentials (2) in momentum representation have the form:

$$V_I^{\bar{\alpha}\bar{\beta}}(k^{\bar{\alpha}}, k'^{\bar{\beta}}) = \sum_{m=1}^{N^{\bar{\alpha}}} \lambda_{(m),I}^{\bar{\alpha}\bar{\beta}} g_{(m),I}^{\bar{\alpha}}(k^{\bar{\alpha}}) g_{(m),I}^{\bar{\beta}}(k'^{\bar{\beta}}). \quad (13)$$

Here for convenience new indices of two-body channels $\bar{\alpha}, \bar{\beta} = 1, 2$ were introduced. Correspondence between a two-body index $\bar{\alpha}$ and a pair (α, i) of three-body channel and Faddeev indices, defining an interacting pair, can be established with the help of Table I of [7]. As before, $N^{\bar{\alpha}}$ defines the number of terms of the potential. As was already stated, we neglected here the πN interaction due to its smallness.

In addition to the coupled-channel potentials (Eq. (13) with $\bar{\alpha}, \bar{\beta} > 1$) we used optical and complex one-channel potentials corresponding to them. Having in mind, that nowadays many authors misuse the term “optical” to a complex potential, we will call our one-channel potentials “exact optical” and “simple complex”. An exact optical potential by definition reproduces the elastic part of the coupled-channel interaction exactly. In particular, the imaginary part of the corresponding amplitude becomes zero below the lowest channel threshold.

Exact optical one-channel potential, corresponding to a two-channel V (with $N^{\bar{\alpha}} = 1$), is given by equation (13) with $\bar{\alpha}, \bar{\beta} = 1$ and the strength parameter defined as

$$\lambda_I^{11, \text{Opt}} = \lambda_I^{11} + \frac{(\lambda_I^{12})^2 \langle g_I^2 | G_0^{(2)}(z^{(2)}) | g_I^2 \rangle}{1 - \lambda_I^{22} \langle g_I^2 | G_0^{(2)}(z^{(2)}) | g_I^2 \rangle}, \quad (14)$$

where $\lambda_I^{\bar{\alpha}, \bar{\beta}}$ are strength parameters of the two-channel potential, $|g_I^2\rangle$ is the form-factor of the second channel. Having in mind, that two-body free Green’s function $G_0^{(2)}$ depends on

the corresponding two-body energy $z^{(2)}$, we see, that $\lambda_I^{11,\text{Opt}}$ of the exact optical potential is an energy-dependent complex function. In contrast to it, a strength parameter $\lambda_I^{11,\text{Complex}}$ of a simple complex potential is a complex constant, therefore, the simple complex potential is energy independent. The strength parameter of a simple complex potential is chosen in such a way, that the potential reproduces some characteristics of the full interaction, say, scattering lengths. Exact optical and simple complex potentials take into account flux losses into inelastic channels through imaginary parts of the strength parameters.

A. $\bar{K}N - \pi\Sigma$ potential

Two versions of phenomenological coupled-channel $\bar{K}N - \pi\Sigma$ potential, constructed in [3], have one- and two-pole form of $\Lambda(1405)$ resonance and simultaneously reproduce all existing experimental data. In the present work we performed new fits of the experimental data with the same potential forms. The one-term ($N^{\bar{\alpha}} = 1$) two-channel potential is defined by Eq. (13), where $\bar{\alpha} = 1$ denotes $\bar{K}N$, $\bar{\alpha} = 2 - \pi\Sigma$ channel. All physical values for data fitting were obtained by solving coupled-channel Lippmann–Schwinger equations with direct inclusion of the Coulomb potential into the K^-p system. Another source of isospin symmetry breaking is the use of physical masses for K^- , \bar{K}^0 , p and n .

In comparison to [3], where one one-pole and one two-pole potentials were constructed, here we obtained two sets of potential parameters $\lambda_I^{\bar{\alpha}\bar{\beta}}$ and $\beta_I^{\bar{\alpha}}$: one set for one-pole and another set for two-pole structure of $\Lambda(1405)$ resonance. Each potential of these sets gives medium value for threshold branching ratios [10, 11]:

$$\gamma = 2.36 \pm 0.04, \quad (15)$$

$$R_{\pi\Sigma} = 0.709 \pm 0.011, \quad (16)$$

where the second is a new ratio, constructed from experimentally measured R_c and R_n :

$$R_{\pi\Sigma} = \frac{R_c}{1 - R_n(1 - R_c)}. \quad (17)$$

In contrast to R_c and R_n , the new branching ratio $R_{\pi\Sigma}$ does not contain the $\pi^0\Lambda$ channel, which is taken into account in our formalism only effectively through the non-zero imaginary part of $\lambda_1^{\bar{K}\bar{K}}$ parameter.

Elastic and inelastic K^-p cross-sections $K^-p \rightarrow K^-p$, $K^-p \rightarrow \bar{K}^0n$, $K^-p \rightarrow \pi^+\Sigma^-$, $K^-p \rightarrow \pi^-\Sigma^+$, and $K^-p \rightarrow \pi^0\Sigma^0$ are properly reproduced by our new potentials as well.

The theoretical results together with experimental data [12–16] are shown in Fig. 1 and Fig. 2 for one- and two-pole sets of potentials, respectively (we did not take into consideration data from [17] with huge error bars). The potentials within each set provide slightly different cross-sections, which results in a band instead of a line in the figures. In the same way as in [3] we defined “total elastic” K^-p cross-section as an integral of the differential cross-section over the $-1 \leq \cos \theta \leq 0.966$ region due to the singularity of the pure Coulomb transition matrix in forward direction.

Characteristics of kaonic hydrogen atom ($\Delta E_{1s}, \Gamma_{1s}$) provided by our potentials are situated within 1σ KEK [18] experimental region, see Fig. 3. Experimental results obtained by DEAR collaboration [19] are also shown. See [44] as well.

Typical resonance behaviour manifests itself in $\pi^0\Sigma^0$ elastic cross-sections, corresponding to one- and two-pole sets of $\bar{K}N - \pi\Sigma$ potential, see Fig. 4 (bands, consisting of individual lines). All resonance maxima are situated near Particle data group (PDG) [22] values for the $\Lambda(1405)$ resonance mass and width

$$M_{\Lambda(1405)}^{PDG} = 1406.5 \pm 4.0 \text{ MeV}, \quad \Gamma_{\Lambda(1405)}^{PDG} = 50 \pm 2.0 \text{ MeV}. \quad (18)$$

PDG mass of the $\Lambda(1405)$ resonance is also shown at the figures. Strong pole positions and widths are slightly different for the potentials within one- and two-pole sets of potentials.

TABLE I: Parameters of the representative one- and two-pole $\bar{K}N - \pi\Sigma$ potentials: range $\beta^{\bar{\alpha}}$ (independent on two-body isospin I), strength $\lambda_I^{\bar{\alpha}\bar{\beta}}$, and additional parameter s of the two-pole model.

	$\beta^{\bar{K}N}$	$\beta^{\pi\Sigma}$	$\lambda_0^{\bar{K}\bar{K}}$	$\lambda_0^{\bar{K}\pi}$	$\lambda_0^{\pi\pi}$	$\lambda_1^{\bar{K}\bar{K}}$	$\lambda_1^{\bar{K}\pi}$	$\lambda_1^{\pi\pi}$	s
$V_{\bar{K}N-\pi\Sigma}^{\text{one-pole}}$	3.41	1.62	-1.2769	0.5586	0.2024	$1.0623 - i0.3251$	1.8315	1.7158	0.0000
$V_{\bar{K}N-\pi\Sigma}^{\text{two-pole}}$	3.72	1.00	-1.6588	0.4672	0.0072	$0.7329 - i0.2967$	1.5357	1.0744	-0.8433

For a more detailed description of the properties of our models of $\bar{K}N - \pi\Sigma$ interaction we chose two “representative” potentials: one with one-pole and another with two-pole structure of $\Lambda(1405)$ resonance. Parameters of the potentials are shown in Table I, the corresponding observables - in Table II. The latter contains the above mentioned γ , $R_{\pi\Sigma}$ ratios

and kaonic hydrogen characteristics ΔE_{1s} , Γ_{1s} together with positions of the strong poles z_1 and z_2 . Potentials with equal z_1 values were chosen as representative ones. The strong K^-p scattering lengths a_{K^-p} , exactly corresponding to the kaonic hydrogen observables, are shown in Table II. Since both a_{K^-p} and $(\Delta E_{1s}, \Gamma_{1s})$ were obtained by exact solution of Lippmann-Schwinger equation, the relation between them does not correspond to any commonly used approximate formula. From Figs. 1, 2, 3 and Table II it is seen, that our new one- and two-pole $\bar{K}N - \pi\Sigma$ potentials reproduce all experimental data within experimental errors indistinguishably well in the same way as the ones in [3]. Therefore it is not possible to give preference to one of the two versions.

TABLE II: Physical characteristics of the representative one-pole and two-pole potentials (full version with physical masses): strong pole(s) position(s) z_1 (and z_2), kaonic hydrogen 1s level shift ΔE_{1s} and width Γ_{1s} , K^-p scattering length a_{K^-p} , and threshold branching ratios γ and $R_{\pi\Sigma}$.

	$V_{\bar{K}N-\pi\Sigma}^{\text{one-pole}}$	$V_{\bar{K}N-\pi\Sigma}^{\text{two-pole}}$
z_1 (MeV)	1409 - i 36	1409 - i 36
z_2 (MeV)	—	1381 - i 105
ΔE_{1s} (eV)	-377	-373
Γ_{1s} (eV)	434	514
a_{K^-p} (fm)	-1.00 + i 0.68	-0.96 + i 0.80
γ	2.36	2.36
$R_{\pi\Sigma}$	0.709	0.709

In addition, we checked several arguments, which were presented in support to the idea of the two-pole structure of $\Lambda(1405)$ resonance. One of them is a difference between charged $\pi\Sigma$ cross-sections, which is seen in different experiments, such as CLAS [23]. In order to check the assumption, that the difference is caused by the two-pole structure, we plotted $\pi^+\Sigma^-$, $\pi^-\Sigma^+$, and $\pi^0\Sigma^0$ elastic cross-sections. The result is seen in Fig. 5: the cross-sections are different and their maxima are shifted one from another for both one- and two-pole versions of $\bar{K}N - \pi\Sigma$ potential. Therefore, it is not a proof of the two-pole structure, but a manifestation of an isospin-breaking effect and different background.

Another argument for two-pole structure comes from the fact, that the poles in a two-pole model are coupled to different channels. Indeed, gradually switching off the coupling between $\bar{K}N$ and $\pi\Sigma$ channels turns the highest of the poles into a real bound state in $\bar{K}N$, while the lowest one become a resonance in uncoupled $\pi\Sigma$ channel. Such a behaviour was demonstrated in several papers, see e.g. [3]. Accordingly, it was suggested, that the poles of a two-body model manifest themselves in different reactions, in particular, $\bar{K}N - \bar{K}N$, $\bar{K}N - \pi\Sigma$, and $\pi\Sigma - \pi\Sigma$ amplitudes should “feel” only one of the two poles. We checked the hypothesis, the results are demonstrated in Fig. 6. Indeed, real parts of $\bar{K}N - \bar{K}N$, $\bar{K}N - \pi\Sigma$, and $\pi\Sigma - \pi\Sigma$ amplitudes in $I = 0$ state cross real axis at different energies, but it is true for both versions of the potential. In fact, the difference is even larger for the one-pole amplitudes. In our opinion, the effect is caused by different background contributions in the reactions independently of the number of poles. Consequently, a proof of the two-pole structure of the $\bar{K}N - \pi\Sigma$ interaction does not exist.

Coulomb interaction, directly included into two-body Lippmann-Schwinger equations, was necessary for reproducing experimental data on kaonic hydrogen atom. However, in the K^-d scattering length calculations it is expected to play a minor role and can be omitted. We also neglected the difference between physical masses in isodoublets for K^-d system. The physical characteristics of $\bar{K}N - \pi\Sigma$ system, calculated with isospin-averaged masses for \bar{K} and N using the obtained sets of $\lambda_I^{\bar{\alpha}\bar{\beta}}$, $\beta_I^{\bar{\alpha}}$ parameters are shown in Fig. 3, Fig. 7, and Table III.

TABLE III: The same as in Table II, but with averaged masses of the particles.

	$V_{\bar{K}N-\pi\Sigma}^{\text{one-pole}}$	$V_{\bar{K}N-\pi\Sigma}^{\text{two-pole}}$
z_1 (MeV)	1409 - i 36	1409 - i 36
z_2 (MeV)	—	1381 - i 105
ΔE_{1s} (eV)	-316	-295
Γ_{1s} (eV)	414	491
a_{K^-p} (fm)	-0.80 + i 0.62	-0.72 + i 0.73
γ	4.18	4.54
$R_{\pi\Sigma}$	0.761	0.768

“Averaged” points $(\Delta E_{1s}, \Gamma_{1s})$ for the one- and two-pole representative potentials in Fig. 3 are shifted to the smaller $|\Delta E_{1s}|$ values relative to the “physical” ones. However, they remain inside 1σ KEK region. Fig. 7 demonstrates “averaged” and “physical” cross-sections, where “averaged” ones naturally do not show threshold behaviour at laboratory momentum P_{lab} , corresponding to $\bar{K}^0 n$ threshold. However, differences between “averaged” and “physical” cross-sections are visible only in the near-threshold region, where there is no reliable experimental data.

Finally, we see by comparing Table III with Table II, that strong pole positions remain almost unchanged. Scattering length a_{K^-p} changes for both versions of the potential mainly due to the confluence of the K^-p and $\bar{K}^0 n$ thresholds into one $\bar{K}N$ threshold. Accordingly, threshold branching ratios γ (15) and $R_{\pi\Sigma}$ (16) are the only observables, which are considerably changed after introducing isospin-averaged masses instead of physical ones.

B. Nucleon-nucleon potentials

Antisymmetrized three-body equations for K^-d system with s -wave interactions contain only spin-triplet NN interaction. We used different NN potentials in order to investigate dependence of the K^-d scattering length on nucleon-nucleon interaction models. One of them is a two-term separable NN potential [24], which reproduces Argonne V18 [25] phase shifts and, therefore, is repulsive at short distances. The potential, which will be called TSA, is described by Eq.(13) with $N^{\bar{\alpha}} = 2$ and $\bar{\alpha} = \bar{\beta} = 1$ (the NN interaction is obviously is diagonal in particle indices). Two versions of the potential (TSA-A and TSA-B) with slightly different form-factors were used:

$$g_{(m)}^{A,NN}(k) = \sum_{n=1}^2 \frac{\gamma_{(m)n}^A}{(\beta_{(m)n}^A)^2 + k^2}, \quad \text{for } (m) = 1, 2 \quad (19)$$

$$g_{(1)}^{B,NN}(k) = \sum_{n=1}^3 \frac{\gamma_{(1)n}^B}{(\beta_{(1)n}^B)^2 + k^2}, \quad g_{(2)}^{B,NN}(k) = \sum_{n=1}^2 \frac{\gamma_{(2)n}^B}{(\beta_{(2)n}^B)^2 + k^2}.$$

TSA-A and TSA-B potentials in the 3S_1 state yield the following scattering lengths and effective radii

$$a^A(np) = -5.402 \text{ fm}, \quad r_{\text{eff}}^A(np) = 1.754 \text{ fm}, \quad (20)$$

$$a^B(np) = -5.413 \text{ fm}, \quad r_{\text{eff}}^B(np) = 1.760 \text{ fm}, \quad (21)$$

and give correct binding energy of the deuteron $E_{\text{deu}} = -2.2246$ MeV.

We also used one-term PEST potential (Eq. (13) with $N^{\bar{\alpha}} = 1$) from Ref. [26], which is a separabelization of the Paris model of NN interaction. The strength parameter of PEST $\lambda = -1$, the form-factor is defined by

$$g_I^{NN}(k) = \frac{1}{2\sqrt{\pi}} \sum_{n=1}^6 \frac{c_{n,I}^{NN}}{k^2 + (\beta_{n,I}^{NN})^2}, \quad (22)$$

where the constants $c_{n,I}^{NN}$ and $\beta_{n,I}^{NN}$ are listed in Ref. [26]. PEST is equivalent to the Paris potential on and off energy shell up to $E_{\text{lab}} \sim 50$ MeV. It reproduces the deuteron binding energy $E_{\text{deu}} = -2.2249$ MeV, as well as the triplet and singlet NN scattering lengths, $a(^3S_1) = -5.422$ fm and $a(^1S_0) = 17.534$ fm, respectively.

The 3S_1 phase shifts for the three NN potentials are shown in Fig. 8 together with characteristics of the Argonne V18 model. Almost indistinguishable lines correspond to the two-term TSA-A and TSA-B potentials, which are very good at reproducing the Argonne V18 phase shifts. Their crossing of the real axis is a consequence of repulsion at short distances. One-term PEST NN potential does not have such a property, but at low energies its phase shifts are also close to the “etalon” ones. Therefore, the two-term NN potentials, increasing the number of equations in a three-body system, reproduce properties of NN interaction better than the one-term potential.

C. $\Sigma N - \Lambda N$ interaction

The ΣN interaction, which is coupled with ΛN channel in $I = \frac{1}{2}$ isospin state, is usually assumed to be spin-dependent [27, 28]. We constructed new versions of $\Sigma N - \Lambda N$ potential in such a way, that it reproduces existing experimental data [29–33]. One-term separable potentials, described by Eq.(13) with $N^{\bar{\alpha}} = 1$ and Yamaguchi form-factors

$$g_{I,S}^{\Sigma N}(k) = \frac{1}{k^2 + (\beta_{I,S}^{\Sigma N})^2} \quad (23)$$

were used for the two possible isospin states. But the number of channels is different for $I = \frac{1}{2}$ and $I = \frac{3}{2}$. The parameters of the one-channel ($\bar{\alpha} = \bar{\beta} = 1$) ΣN interaction with isospin $I = \frac{3}{2}$ were fitted to the $\Sigma^+ p \rightarrow \Sigma^+ p$ cross-sections. Isospin one-half ΣN is coupled to ΛN channel, therefore, at first we constructed a coupled-channel potential of the $I = \frac{1}{2}$ $\Sigma N - \Lambda N$ interaction. The channel indices $\bar{\alpha}, \bar{\beta} = 1, 2$ in (13) denote ΣN and ΛN channel,

correspondingly. The coupled-channel $I = \frac{1}{2}$ potential together with the one-channel $I = \frac{3}{2}$ potential reproduces the $\Sigma^- p \rightarrow \Sigma^- p$, $\Sigma^- p \rightarrow \Sigma^0 n$, $\Sigma^- p \rightarrow \Lambda n$, and $\Lambda p \rightarrow \Lambda p$ cross-sections.

TABLE IV: Range $\beta^{\bar{\alpha}}$ (independent on two-body isospin I) and strength $\lambda_I^{\bar{\alpha}\bar{\beta}}$ parameters of the two $\Sigma N - \Lambda N$ potentials: V_S^{Sdep} and V^{Sind} (S stands for the spin). Scattering lengths $a_I^{\bar{\alpha}}$ of ΣN and ΛN systems are also shown (in fm).

	$\beta^{\Sigma N}$	$\lambda_{\frac{3}{2}}^{\Sigma N}$	$\beta^{\Lambda N}$	$\lambda_{\frac{1}{2}}^{\Sigma \Sigma}$	$\lambda_{\frac{1}{2}}^{\Sigma \Lambda}$	$\lambda_{\frac{1}{2}}^{\Lambda \Lambda}$	$a_{\frac{1}{2}}^{\Sigma N}$	$a_{\frac{3}{2}}^{\Sigma N}$	$a_{\frac{1}{2}}^{\Lambda N}$
$V_{S=0}^{\text{Sdep}}$	1.25	-0.0244	0.62	-1.9956	1.1408	-0.7148	$-1.90 + i 0.08$	3.18	1.26
$V_{S=1}^{\text{Sdep}}$	0.50	-0.0007	1.03	-0.0008	0.0185	0.0000	$-3.17 + i 1.30$	1.63	1.57
V^{Sind}	0.74	-0.0032	0.74	-0.0011	0.0254	0.0190	$-2.40 + i 0.85$	1.95	-1.47

Two versions of $I = \frac{1}{2}$ $\Sigma N - \Lambda N$ and $I = \frac{3}{2}$ ΣN potentials were constructed: one is spin dependent V^{Sdep} , the other V^{Sind} is independent of spin. Both perfectly reproduce all existing experimental data [29–33] on ΣN and ΛN cross-sections, as is seen in Fig. 9. Parameters of the potentials are shown in Table IV together with scattering length values $a_{\frac{1}{2}}^{\Sigma N}$, $a_{\frac{3}{2}}^{\Sigma N}$, and $a_{\frac{1}{2}}^{\Lambda N}$. The scattering lengths of spin dependent potential V^{Sdep} are in qualitative agreement with those provided by more complicated models of ΣN interaction [27, 28]. The only exception is $a_{\frac{3}{2}}^{\Sigma N}$ with $S = 1$, having opposite sign, which, however, is the same as that given in previous versions of the same advanced potentials (our definition of the sign of a scattering length is opposite to those, used in the mentioned articles). The scattering lengths, of the spin independent potential V^{Sind} , are not in such a good agreement, but having in mind, that the scattering length is not a directly measurable quantity, we do not consider this difference as a serious defect.

For the three-body K^-d calculations, however, where a channel containing Λ is not included directly, we need not a coupled-channel, but a one-channel ΣN model of interaction in $I = \frac{1}{2}$ state. Due to this, we additionally constructed an exact optical $V^{\Sigma N, \text{Opt}}$ and simple complex $V^{\Sigma N, \text{Complex}}$ potentials, corresponding to the obtained $I = \frac{1}{2}$ $\Sigma N - \Lambda N$ potential. As was discussed at the beginning of the Section III, the exact optical potential has an energy dependent strength parameter defined by Eq. (14) and exactly reproduces the elastic ΣN

amplitude of the corresponding two-channel potential. Parameters of the $V^{\Sigma N, \text{Complex}}$ were found in such a way, that the simple complex potential gives the same scattering lengths, as the two-channel potential. Thus, the exact optical and the simple complex $\Sigma N(-\Lambda N)$ potentials in $I = \frac{1}{2}$ state and the one-channel ΣN potential in $I = \frac{3}{2}$ were used during three-body calculations. The second channel in brackets $(-\Lambda N)$ underlines, that the one-channel potentials correspond to the coupled-channel one.

IV. APPROXIMATE METHODS

Apart from the full coupled-channel calculation, we performed checks of several approximate methods, usually used for K^-d scattering length problem, as well. It is obvious, that a comparison between the full and approximate results is meaningful only if it is performed with equal two-body input.

A. One-channel AGS calculations

In order to investigate the importance of direct inclusion of $\pi\Sigma N$ channel we performed one-channel AGS calculations as well. It means, that we solved Eq. (10) with $\alpha = \beta = 1$, thus, only $\bar{K}N$ and NN T -matrices enter the equations. We constructed the exact optical and two simple complex one-channel $\bar{K}N(-\pi\Sigma)$ potentials approximating the full coupled-channel one- and two-pole models of interaction. As mentioned at the beginning of Section III, the exact optical potential $V^{\bar{K}N, \text{Opt}}$ provides exactly the same elastic $\bar{K}N$ amplitude as the coupled-channel model of interaction. Its energy-dependent strength parameters are defined by Eq. (14) with $\bar{\alpha}, \bar{\beta} = 1, 2$ stands for $\bar{K}N$ and $\pi\Sigma$ channels, correspondingly.

For the simple complex potentials we used range parameters $\beta^{\bar{K}N}$ of the coupled-channel $\bar{K}N - \pi\Sigma$ models of interaction. The complex $\lambda_I^{11, \text{Complex}}$ constants were obtained in two ways. The first version of the simple complex $\bar{K}N$ potential $V_{(a,z)}^{\bar{K}N, \text{Complex}}$ reproduces K^-p scattering length a_{K^-p} and pole position z_1 of the corresponding coupled-channel version of the potential, shown in Table III. The second one, $V_{(a,a)}^{\bar{K}N, \text{Complex}}$ provides the same $I = 0$ and $I = 1$ isospin $\bar{K}N$ scattering lengths as the full $\bar{K}N - \pi\Sigma$:

$$a_{\bar{K}N, I=0}^{\text{one-pole}} = -1.60 + i 0.67 \text{ fm}, \quad a_{\bar{K}N, I=0}^{\text{two-pole}} = -1.62 + i 0.78 \text{ fm}, \quad (24)$$

$$a_{\bar{K}N, I=1}^{\text{one-pole}} = -0.004 + i 0.57 \text{ fm}, \quad a_{\bar{K}N, I=1}^{\text{two-pole}} = 0.18 + i 0.68 \text{ fm}. \quad (25)$$

B. Fixed center approximation

So-called “Fixed center approximation to Faddeev equations” (FCA) introduced in [34] is a variant of FSA or a two-center formula. Fixed-scatterer approximation (FSA) or a two-center problem assumes, that the scattering of a projectile particle takes place on two much heavier target particles separated by a fixed distance. The motion of the heavy particles is subsequently taken into account by averaging the obtained projectile-target amplitude over the bound state wave function of the target. Therefore, the approximation is well-known and works properly in atomic physics, where an electron is really much lighter than a nucleon or an ion. Having in mind, that the antikaon mass is only twice smaller than the mass of a nucleon, we can expect, that FSA hardly can be a good approximation for the K^-d scattering length calculation.

The FCA formula was obtained in [34] from Faddeev equations in a very strange way. Proper derivation of a FSA formula starting from the same equations was done much earlier in [35], it can also be found in [36] together with several versions of the FSA formula. Fixed scatterer approximation for the calculation of a_{K^-d} scattering length using separable potentials was used in [37].

A novelty of the FCA formula of [34] is introduction of “isospin breaking terms”, which, according to the authors, come from \bar{K}^0n two-body particle channel introduced in addition to K^-p . However, the inclusion of the \bar{K}^0n channel is questionable, since, as it was already mentioned in Section II, all terms, connected with this subsystem, automatically drop out from the Faddeev system of equations after antisymmetrization.

Necessity to go beyond FCA formula for the K^-d system was clearly demonstrated in [38], where the unstable character of the FCA results was pointed out. However, the formula is still being used, for example in [39], that is why we decided to check the approximation. We used the same two-body input as in AGS equations in order to make the comparison as adequate as possible.

First of all, we used the scattering lengths provided by our coupled-channel $\bar{K}N - \pi\Sigma$ potentials and the deuteron wave function corresponding to our TSA-B NN potential in FCA formula Eq.(24) from [34]. Secondly, all \bar{K}^0n parts were removed from the formula because they do not enter AGS equations. Finally, we took into account the fact, that the FCA formula was obtained for a local $\bar{K}N$ potential, while separable $\bar{K}N - \pi\Sigma$ potentials

were used in our Faddeev equations. The corresponding changes in the FCA formula were made [45]. Therefore, the two-body input for the FCA formula was equivalent to the input for the AGS calculation.

V. RESULTS AND DISCUSSION

The results of the full coupled-channel calculations of the K^-d scattering length using sets of one- (empty circles) and two-pole (empty squares) versions of the coupled-channel $\bar{K}N - \pi\Sigma$ potentials are shown in Fig.10. The calculations were performed with V_{NN}^{TSA-B} and exact optical $V_{\Sigma N}^{\text{Sdep,Opt}}$. The K^-p scattering length values obtained with the two representative $\bar{K}N - \pi\Sigma$ potentials are:

$$a_{K^-d}^{\text{one-pole}} = -1.49 + i 0.98 \text{ fm}, \quad (26)$$

$$a_{K^-d}^{\text{two-pole}} = -1.57 + i 1.11 \text{ fm}. \quad (27)$$

Results of previous Faddeev calculations of the same system (filled squares) together with two FCA results (crossed squares) are also shown in the figure.

It is seen, that while two-body data do not allow to distinguish between one- and two-pole versions of “the main” $\bar{K}N - \pi\Sigma$ interaction, the three-body sets of results differ sufficiently for such a task. Therefore, in principle, it would be possible to favor one version of the $\bar{K}N - \pi\Sigma$ potential by comparing with an experimental result. However, direct measurement of K^-d scattering length is impossible. Moreover, it is not absolutely clear, whether the difference between the two sets of the a_{K^-d} results is much more than theoretical uncertainties, caused mainly by the uncertainties of the $\bar{K}N$ model of interaction. In any case, a calculation of $1s$ level shift $\Delta E_{\text{deu},1s}$ and width $\Gamma_{\text{deu},1s}$ of kaonic deuterium atom, corresponding to the obtained a_{K^-d} values, is necessary for comparing with experimentally measurable values. The parameters of kaonic deuterium were being measured by SIDDHARTA experiment, unfortunately, without any results. Due to this our next step will be making predictions for $\Delta E_{\text{deu},1s}$ and $\Gamma_{\text{deu},1s}$ observables.

As is seen in Fig 10, our a_{K^-d} results are close to the other K^-d scattering lengths obtained in [40] and [41] within coupled-channel Faddeev approach. The result of [42], obtained by a one-channel Faddeev calculation with a zero-range one-channel $\bar{K}N$ potential, has much smaller absolute value of the real part than all other a_{K^-d} . On the contrary, the

authors of [38], who performed Faddeev calculations using NN interaction with d -wave component, obtained K^-d scattering length with quite larger absolute values of both real and imaginary parts.

The a_{K^-d} value of [34], significantly different from all others, was calculated using the FCA formula, obtained in the same paper and already discussed in Section IV B. We chose the result calculated in isospin basis for the comparison. One more paper, where FCA formula was used, is [39], where, however, the result was obtained by simply applying of two approximate formulae. The second one is the corrected Deser formula, used for calculation of the $\bar{K}N$ scattering lengths, entering the FCA. One of the representative a_{K^-d} values from [39], having the largest possible imaginary part, is shown in Fig.10.

It is hard to compare all a_{K^-d} results, because the methods of treatment of the three-body problem and two-body inputs are different in the mentioned works. In order to investigate separate effects of several approximations we performed approximate calculations, as described in Section IV. The obtained one-channel AGS a_{K^-d} values (Section IV A) together with FCA (Section IV B) and the representative coupled-channel AGS results of the K^-d scattering length calculations are shown in Fig. 11 for one- and two-pole versions of $\bar{K}N - \pi\Sigma$ interaction. It is important, that all results in the figure were obtained with equivalent two-body input, including the neglect of isospin-breaking parts in the original FCA formula.

It is seen from Fig.11, that all approximations are more accurate for the one-pole version of the $\bar{K}N$ interaction than for the two-pole variant. The one-channel AGS calculation with exact optical $\bar{K}N$ potential (empty symbols), giving exactly the same $\bar{K}N - \bar{K}N$ amplitude as the corresponding coupled-channel potential, turns out to be the best approximation. The result, obtained with the simple complex potential $V_{(a,a)}^{\bar{K}N,\text{complex}}$ (vertically crossed symbols), reproducing $I = 0$ and $I = 1$ $\bar{K}N$ scattering lengths, underestimates the absolute value of the real part of the a_{K^-d} , especially for the two-pole version of $\bar{K}N$ interaction, but have rather accurate imaginary part of the K^-d scattering length. Another one-channel AGS calculation with simple complex potential $V_{(a,z)}^{\bar{K}N,\text{complex}}$, reproducing K^-p scattering length and pole position z_1 , gives rather inaccurate result (half-empty symbols) as compared with the coupled-channel AGS values (filled symbols).

The scattering length a_{K^-d} of [42] was obtained from one-channel Faddeev equations with a complex potential. However, the underestimation of the absolute values of its real part in comparison to other Faddeev calculations is so large, that it cannot be explained

by the method only. The most likely reason of the difference lies in the properties of the $\bar{K}N$ potential used in [42]. First of all, the potential has a very large mass of the K^-p quasibound state (1439 MeV), which, therefore, is situated above the K^-p threshold. In addition, the width of the state (127 MeV) is much larger than the PDG value (50 MeV) as well as the width of our z_1 pole (72 MeV).

It is hard to understand the results obtained in [38]. While all formulae are written for many-channel Faddeev equations, the most of the dependences and even “the best” a_{K-d} value were obtained within a one-channel Faddeev calculation including $\bar{K}N$ and NN interactions only. Since the elastic part of the coupled-channel $\bar{K}N$ T -matrix was used, the result is equivalent to a one-channel Faddeev calculation with an exact optical potential. But even the full coupled-channel calculation was performed in [38] with non-unitary $\bar{K}N$ T -matrices OSA and OS1, since channels with η -mesons, entering the two-body T , were omitted in the three-body equations. It is not clear, why the one-channel calculations of [38] give so large difference in imaginary parts of a_{K-d} obtained in isospin and particle basis and with and without d -wave in NN . The result of a calculation, in principle, should not depend on the chosen basis, in addition, the very recent results of K^-d scattering calculations [43] demonstrated, that inclusion of physical masses into Faddeev equations change a_{K-d} by several percents only.

The results of using the FCA formula without isospin-breaking effects (crossed symbols) stays far away from the full calculation, as is seen in Fig.11. While errors for the imaginary part are not so large, the module of the real part is underestimated by about 30%. Therefore, our calculations show, that FCA is a poor approximation for K^-d scattering length calculation, and the accuracy is lower for the two-pole $\bar{K}N$ model of interaction (the most of chirally-based models of $\bar{K}N$ interaction have two-pole structure). Even the original FCA formula does not give such a large K^-d scattering length as a_{K-d} from [34], which, therefore, is caused by too large input $\bar{K}N$ scattering lengths. As for the values of [39], they suffer from cumulative errors of two approximations and using of DEAR results on kaonic hydrogen characteristics. As was shown in [3], the error of the corrected Deser formula makes about 10%, while the problems with DEAR experimental data were also demonstrated in the paper and in other theoretical works.

We investigated dependence of the full coupled-channel results on NN and $\Sigma N(-\Lambda N)$ interactions as well. The dependence of a_{K-d} on nucleon-nucleon interaction is demonstrated

in Fig 12, were the results obtained with TSA-A, TSA-B, and PEST V^{NN} , are shown. The representative sets of one- and two-pole $\bar{K}N - \pi\Sigma$ potentials were used together with exact optical $V^{\text{Sdep,Opt}} \Sigma N(-\Lambda N)$ model of interaction. We see from the Figure, that the difference is very small even for the potentials with and without repulsion at short distances (TSA and PEST, correspondingly). Therefore, the s -wave NN interaction, which is used in the present calculation, plays minor role in the calculation. Most likely, it is caused by relative weakness of the NN interaction as compared to $\bar{K}N$ from the viewpoint of a much deeper quasibound state in the latter system ($E_{\bar{K}N} \approx -23$ MeV for our potentials) than the deuteron bound state ($E_{\text{deu}} \approx -2$ MeV). We do not expect much larger effect from higher partial waves in NN as well.

We also looked at the dependence of a_{K^-d} on $\Sigma N(-\Lambda N)$ interaction. The K^-d scattering lengths obtained with the exact optical and the simple complex versions of the spin dependent V^{Sdep} and spin independent V^{Sind} potentials are shown in Fig. 13. The representative sets of one- and two-pole $\bar{K}N - \pi\Sigma$ potentials were used together with TSA-B NN potential. The results of the two versions of $\Sigma N(-\Lambda N)$ potential V^{Sdep} and V^{Sind} in exact optical form are very close, while their simple complex versions are slightly different. However, the largest error does not exceed 3%, therefore, the dependence of the a_{K^-p} on $\Sigma N - (\Lambda N)$ interaction is also weak.

VI. CONCLUSIONS

To conclude, we performed calculations of the K^-d scattering length using newly obtained coupled-channel $\bar{K}N - \pi\Sigma$ potentials with one- and two-pole versions of the $\Lambda(1405)$ resonance. Faddeev-type AGS equations were used for description of $\bar{K}NN - \pi\Sigma N$ system. We also constructed new coupled-channel $\Sigma N - \Lambda N$ potentials together with its exact optical and simple complex $\Sigma N(-\Lambda N)$ versions. Different models of the NN interaction: TSA-A, TSA-B, and PEST were used. All two-body interactions are described by s -wave separable potentials. We investigated dependence of a_{K^-d} on NN and $\Sigma N(-\Lambda N)$ interaction and found, that both dependences are weak.

We found, that the two sets of the results, obtained with one- and two-pole models of $\Lambda(1405)$ resonance, are clearly separated one from another, in principle, allowing to give preference to one of the $\bar{K}N - \pi\Sigma$ interaction models. However, the question, whether

theoretical uncertainties are not of the same order as the differences between the two obtained sets of a_{K^-d} , remains open. In any case, it is necessary to calculate level shifts and widths of kaonic deuterium atom, corresponding to the obtained K^-d scattering lengths, which can be measured, say, by SIDDHARTA-2 experiment. It is assumed to be done in a next paper.

Among approximate results, the one-channel AGS calculation with exact optical $\bar{K}N(-\pi\Sigma)$ potential gives the best approximation to the full coupled-channel result. On the contrary, FCA was shown to be the least accurate approximation, especially in reproduction of the real part of the K^-d scattering length. All approximations are less accurate for the two-pole model of $\bar{K}N - \pi\Sigma$ interaction.

Acknowledgments. The author is thankful to J. Révai for many fruitful discussions and to J. Haidenbauer for his comments concerning $\Sigma N - \Lambda N$ interaction. The work was supported by the Czech GA AVCR grant KJB100480801.

-
- [1] Mini-Proceedings ECT* Workshop "Hadronic Atoms and Kaonic Nuclei", (ECT*, Trento, Italy, October 12–16, 2009), Eds. C. Curceanu and J. Marton; nucl-ex/1003.2328.
 - [2] L.D. Faddeev, Soviet Phys. JETP 12, 1014 (1961); Mathematical aspects of the three-body problem in quantum scattering theory, Steklov Math. Institute 69 (1963).
 - [3] J. Révai, N.V. Shevchenko, Phys. Rev. C 79, 035202 (2009).
 - [4] C. Curceanu *et al.*, Eur. Phys. J. A 31, 537 (2007).
 - [5] E.O. Alt, P. Grassberger, W. Sandhas, Nucl. Phys. B 2, 167 (1967).
 - [6] N.V. Shevchenko, A. Gal, J. Mareš, Phys. Rev. Lett. 98, 082301 (2007).
 - [7] N.V. Shevchenko, A. Gal, J. Mareš, J. Révai, Phys. Rev. C 76, 044004 (2007).
 - [8] V.B. Belyaev, *Lectures on the Theory of Few-Body Systems*, (Springer Verlag, 1990).
 - [9] F. Sohre and H. Ziegelman, Phys. Lett. B 34, 579 (1971).
 - [10] D.N. Tovee *et al.*, Nucl. Phys. B 33, 493 (1971).
 - [11] R.J. Nowak *et al.*, Nucl. Phys. B 139, 61 (1978).
 - [12] M. Sakitt *et al.*, Phys. Rev. 139, B719 (1965).
 - [13] J.K. Kim, Phys. Rev. Lett. 14, 29 (1965); Columbia University Report, Nevis, 149 (1966); Phys. Rev. Lett. 19, 1074 (1967).

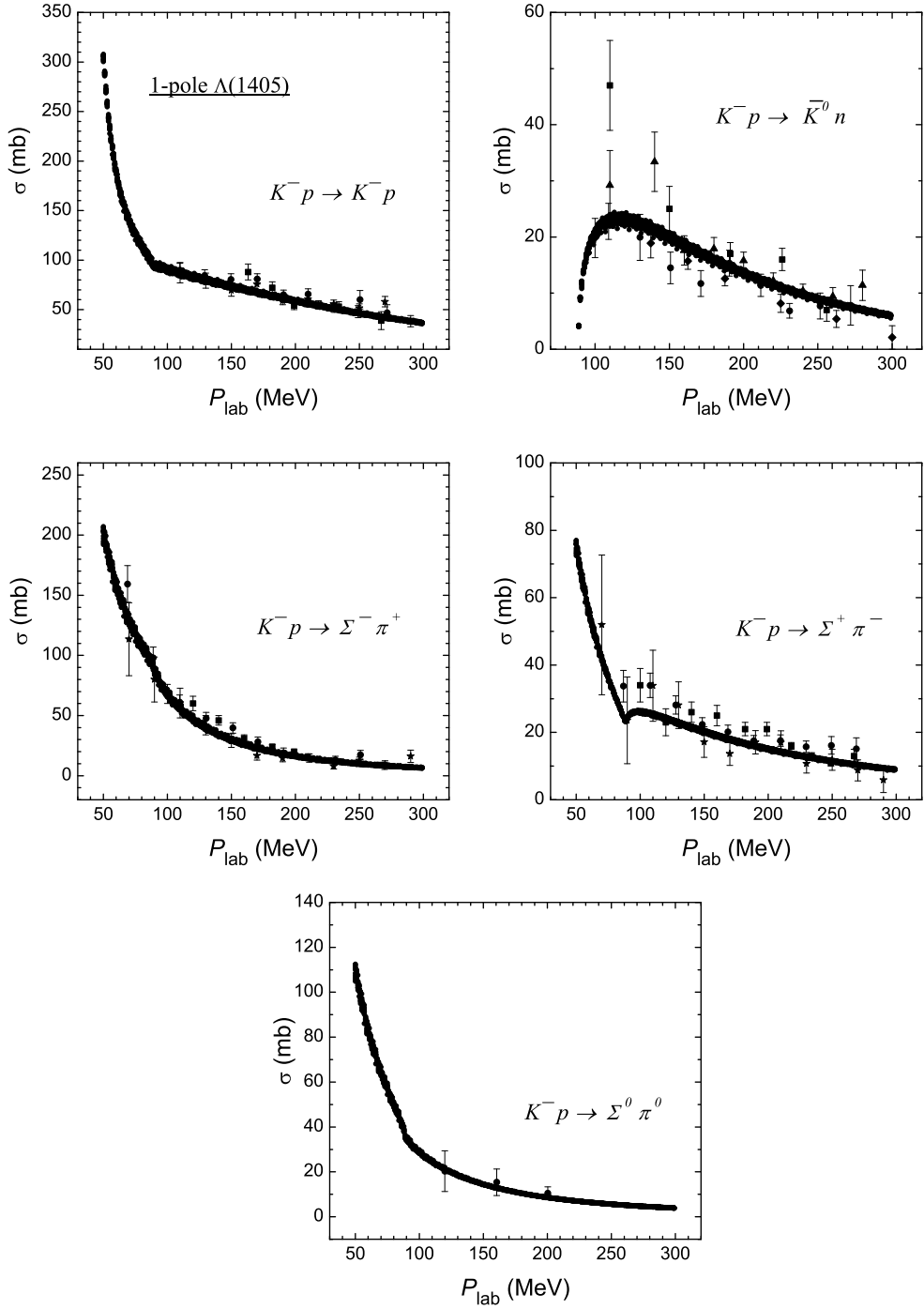


FIG. 1: Comparison of the elastic and inelastic K^-p cross-sections (filled circles) for the one-pole sets of the $\bar{K}N - \pi\Sigma$ potential with experimental data [12–16] (data points). The theoretical bands are formed by all lines obtained with individual potentials within the set.

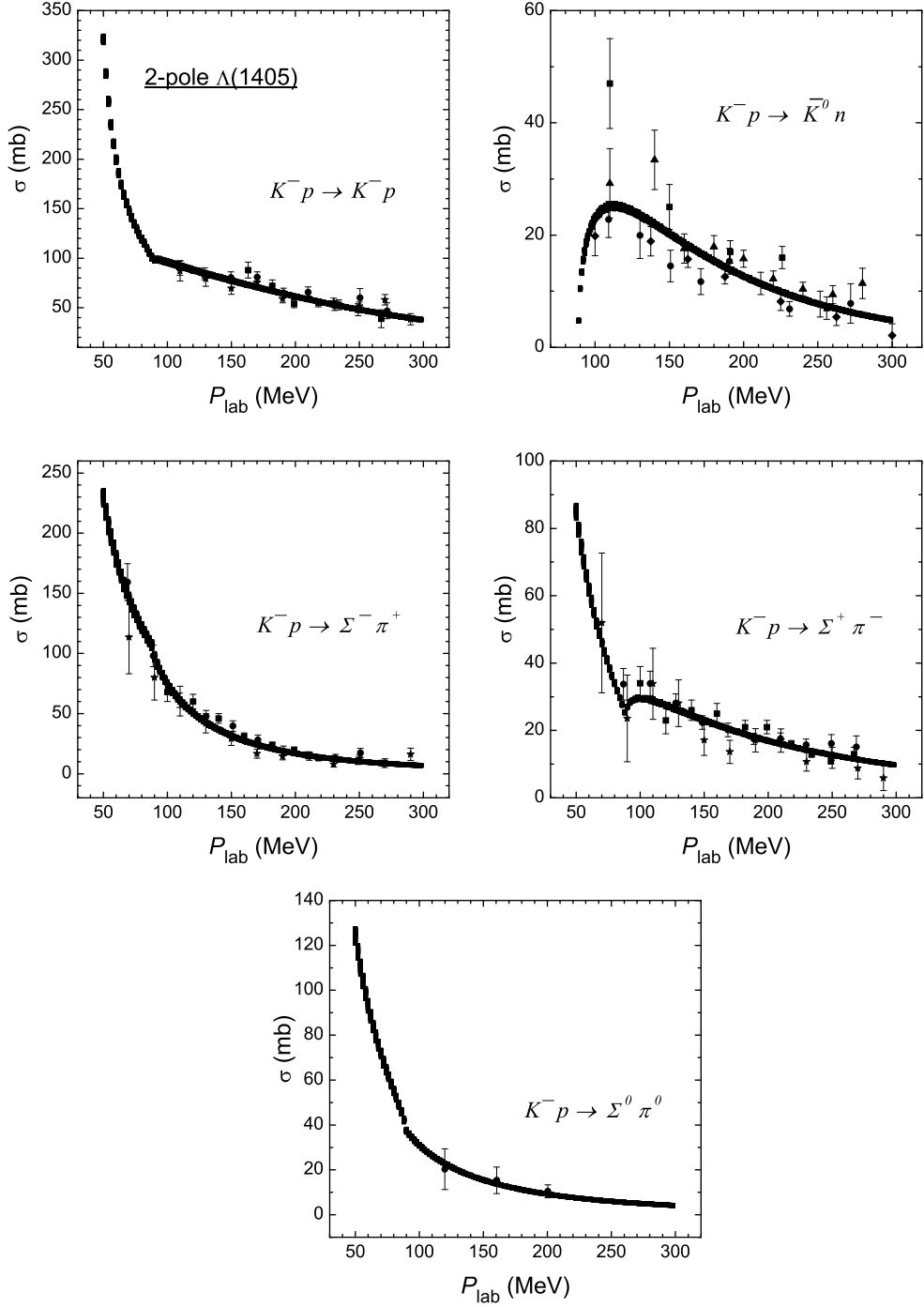


FIG. 2: Comparison of the elastic and inelastic K^-p cross-sections (filled circles) for the two-pole sets of the $\bar{K}N - \pi\Sigma$ potential with experimental data [12–16] (data points). The theoretical bands are formed by all lines obtained with individual potentials within the set.

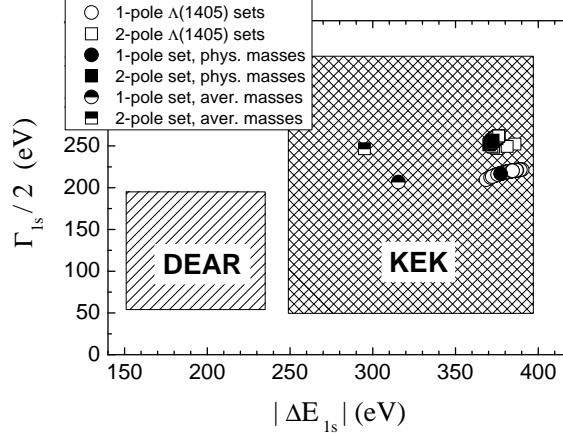


FIG. 3: Kaonic hydrogen 1s level shift $|\Delta E|$ (absolute value) and width Γ values for the one-pole (empty circles) and two-pole (empty squares) sets of the $\bar{K}N - \pi\Sigma$ potential. Filled circle and filled square denote the results for the one- and two-pole representative potentials, correspondingly, obtained with physical masses. The same kaonic hydrogen observables calculated with averaged masses are denoted by half-empty circle and square. Experimental DEAR and KEK 1σ confidence regions are also shown.

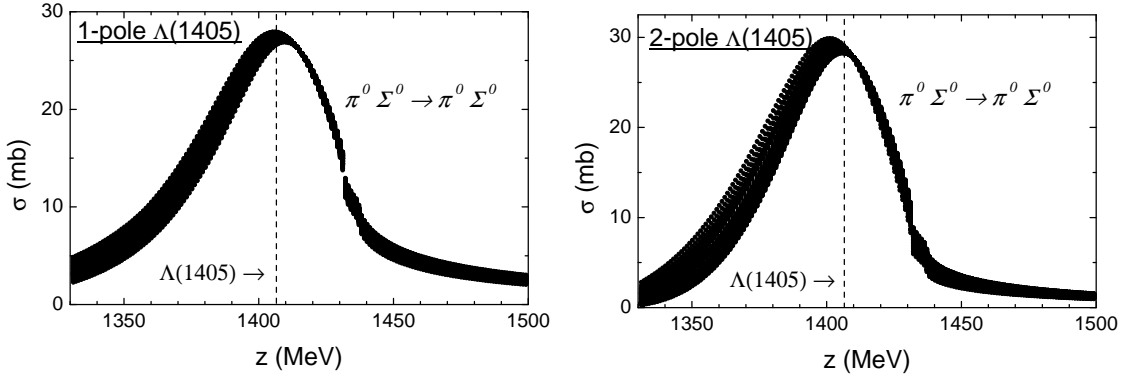


FIG. 4: Elastic $\pi^0\Sigma^0$ cross-sections for the one-pole (left) and two-pole sets of $\bar{K}N - \pi\Sigma$ potential. The theoretical bands are formed by all lines obtained with individual potentials within the corresponding set.

[14] W. Kittel, G. Otter, and I. Wacek, Phys. Lett. 21, 349 (1966).

[15] J. Ciborowski *et al.*, J. Phys. G 8, 13 (1982).

[16] D. Evans *et al.*, J. Phys. G 9, 885 (1983).

[17] W.E. Humphrey, R.R. Ross, Phys. Rev. 127, 1305 (1962).

[18] M. Iwasaki *et al.*, Phys. Rev. Lett. 78, 3067 (1997); T.M. Ito *et al.*, Phys. Rev. C 58, 2366 (1998).

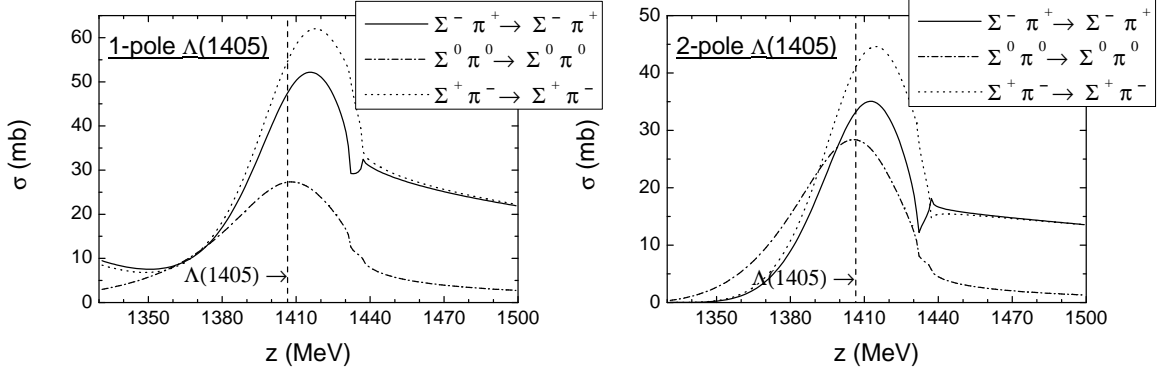


FIG. 5: Three charged elastic $\pi\Sigma$ cross-sections for the representative one-pole (left) and two-pole $\bar{K}N - \pi\Sigma$ potentials.

- [19] G. Beer *et al.*, Phys. Rev. Lett. 94, 212302 (2005).
- [20] M. Bazzi *et al.*, nucl-ex/1105.3090.
- [21] B. Borasoy, U.-G. Meißner, R. Niffler, Phys. Rev. C 74, 055201 (2006).
- [22] K. Nakamura *et al.* (Particle Data Group), J. Phys. G 37, 075021 (2010).
- [23] R. Schumacher (for the CLAS Collaboration), AIP Conf. Proc. 1257, 100 (2010).
- [24] P. Doleschall, *private communication*.
- [25] R. B. Wiringa, V. G. J. Stoks, and R. Schiavilla, Phys. Rev. C 51, 38 (1995).
- [26] H. Zankel, W. Plessas, J. Haidenbauer, Phys. Rev. C 28, 538 (1983).
- [27] J. Haidenbauer, U.-G. Meissner, Phys. Rev. C 72, 044005 (2005).
- [28] Th. A. Rijken, Y. Yamamoto, Phys. Rev. C 73, 044008 (2006).
- [29] G. Alexander, U. Karshon, A. Shapira, G. Yekutieli, R. Engelmann, H. Filthuth, and W. Lughofer, Phys. Rev. 173, 1452 (1968).
- [30] B. Sechi-Zorn, B. Kehoe, J. Twitty, and R. A. Burnstein, Phys. Rev. 175, 1735 (1968).
- [31] F. Eisele, H. Filthuth, W. Fölisch, V. Hepp, E. Leitner, and G. Zech, Phys. Lett. B 37, 204 (1971).
- [32] R. Engelmann, H. Filthuth, V. Hepp, and E. Kluge, Phys. Lett. 21, 587 (1966).
- [33] V. Hepp and M. Schleich, Z. Phys. 214, 71 (1968).
- [34] S.S. Kamalov, E. Oset, A. Ramos, Nucl. Phys. A 690, 494 (2001).
- [35] V.V. Peresypkin, Ukr. Fiz. Zh. 23, 1256 (1978).
- [36] A. Deloff, *Fundamentals in hadronic atom theory*, (World scientific, 2003).
- [37] R. C. Barrett, A. Deloff, Phys. Rev. C 60, 025201 (1999).

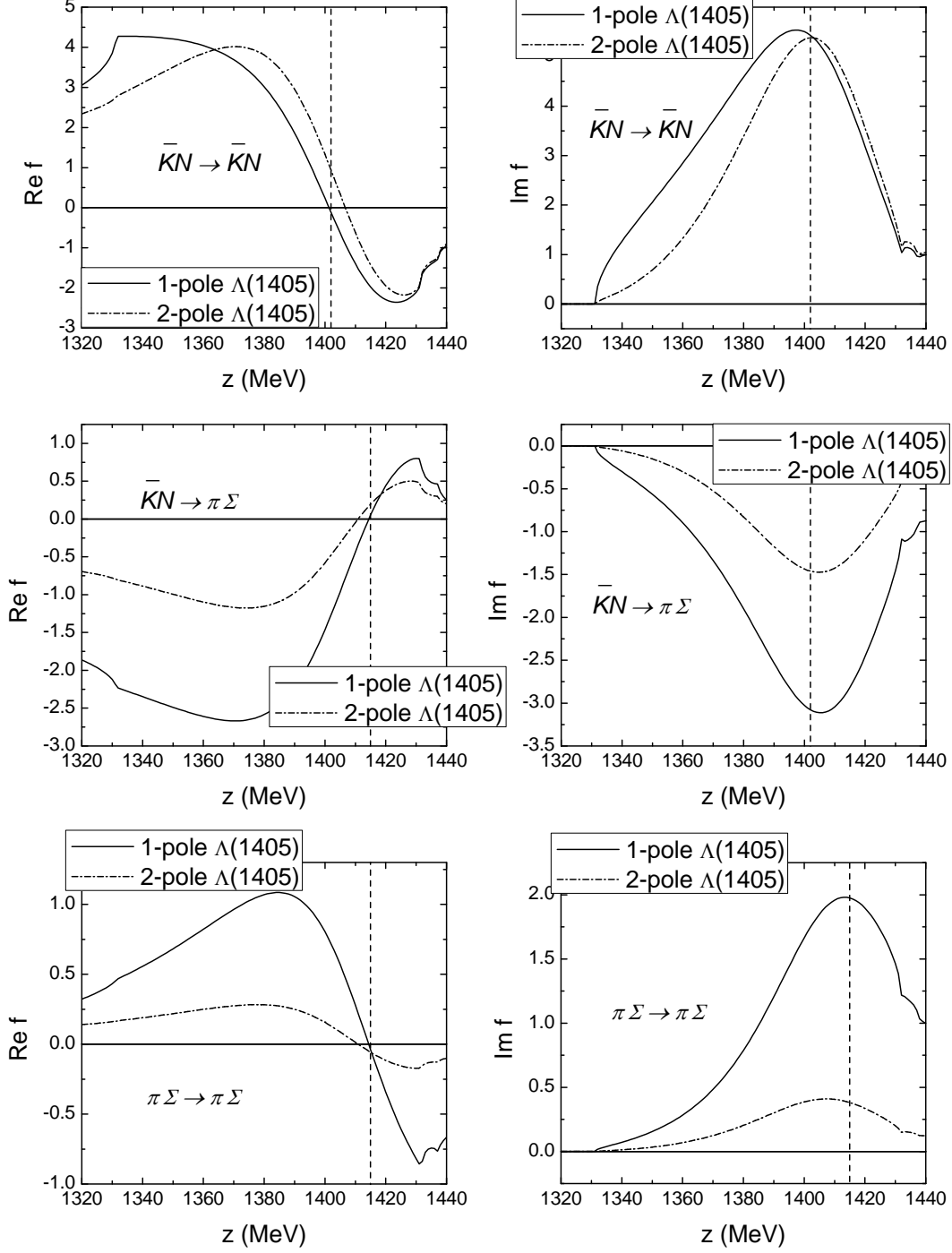


FIG. 6: Real (left column) and imaginary (right column) parts of the $\bar{K}N - \bar{K}N$, $\bar{K}N - \pi\Sigma$ and $\pi\Sigma - \pi\Sigma$ amplitudes obtained with one-pole (solid line) and two-pole (dash-dotted line) representative $\bar{K}N - \pi\Sigma$ potentials. The energies at which real parts of the one-pole amplitudes cross real axes are denoted by vertical dashed lines.

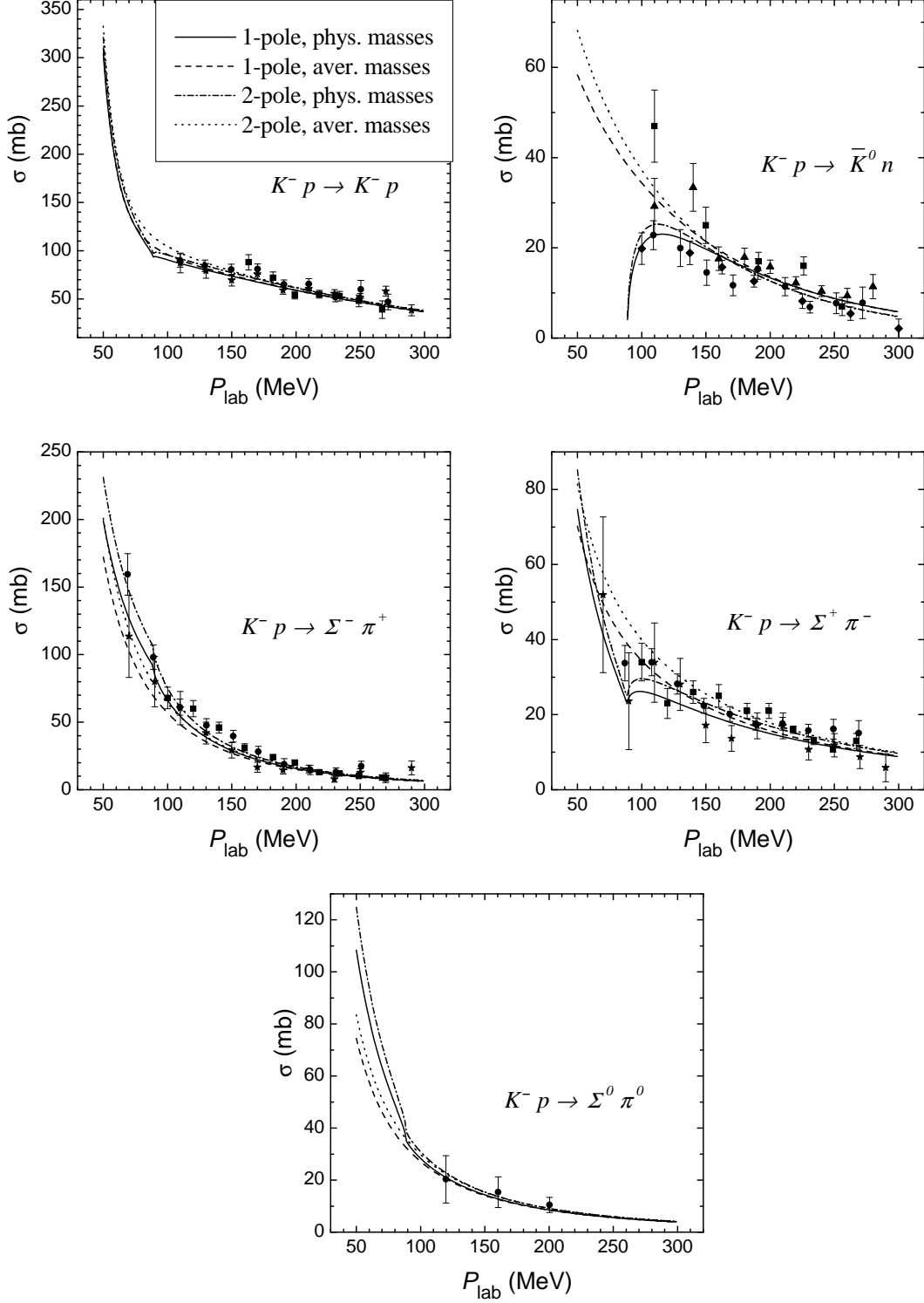


FIG. 7: Comparison of the theoretical $K^- p$ cross-sections for the representative one- and two-pole $\bar{K}N - \pi\Sigma$ potentials with experimental data [12–16] (data points). The results obtained with the physical masses (solid, dash-dotted line) and the averaged masses (dashed and dotted line) are presented.

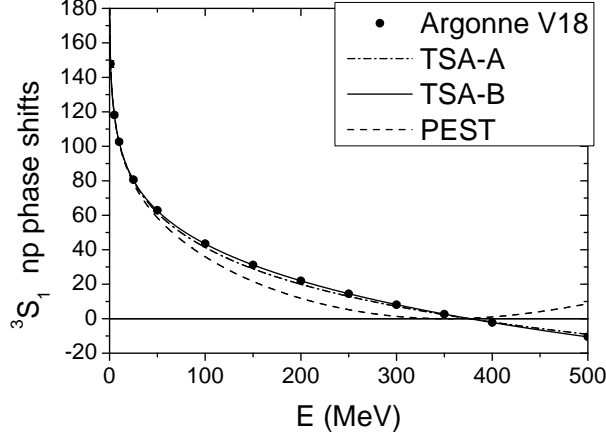


FIG. 8: 3S_1 np phase shifts of TSA-A (dash-dotted line), TSA-B (solid line), and PEST (dashed line) NN potentials in comparison with those of Argonne *v18* potential (solid circles).

[38] A. Bahaoui, C. Fayard, T. Mizutani, B. Saghai, Phys. Rev. C 68, 064001 (2003).

[39] U.-G. Meissner, U. Raha, A. Rusetsky, Eur. Phys. J. C 47, 473 (2006).

[40] G. Toker, A. Gal, J.M. Eisenberg, Nucl. Phys. A 362, 405 (1981).

[41] M. Torres, R.H. Dalitz, A. Deloff, Phys. Lett. B 174, 213 (1986).

[42] A. Deloff, Phys. Rev. C 61, 024004 (2000).

[43] J. Révai, *to be published*.

[44] After sending the present article to the journal the results of SIDDHARTA experiment appeared, see [20]. The 1σ SIDDHARTA region is situated inside KEK square with comparable width Γ_{1s} and smaller level shift ΔE_{1s} values than those provided by our potentials.

[45] To remove the difference we used $G(R)$ function defined by Eq.(25) in [37] instead of $1/R$ function, which is an approximation of the $G(R)$, in the FCA formula. The range parameter $\beta^{\bar{K}N}$, entering the $G(R)$ function, was also taken from our coupled-channel $\bar{K}N-\pi\Sigma$ potential. In fact, the replacement $1/R$ by $G(R)$ changed the results negligibly.

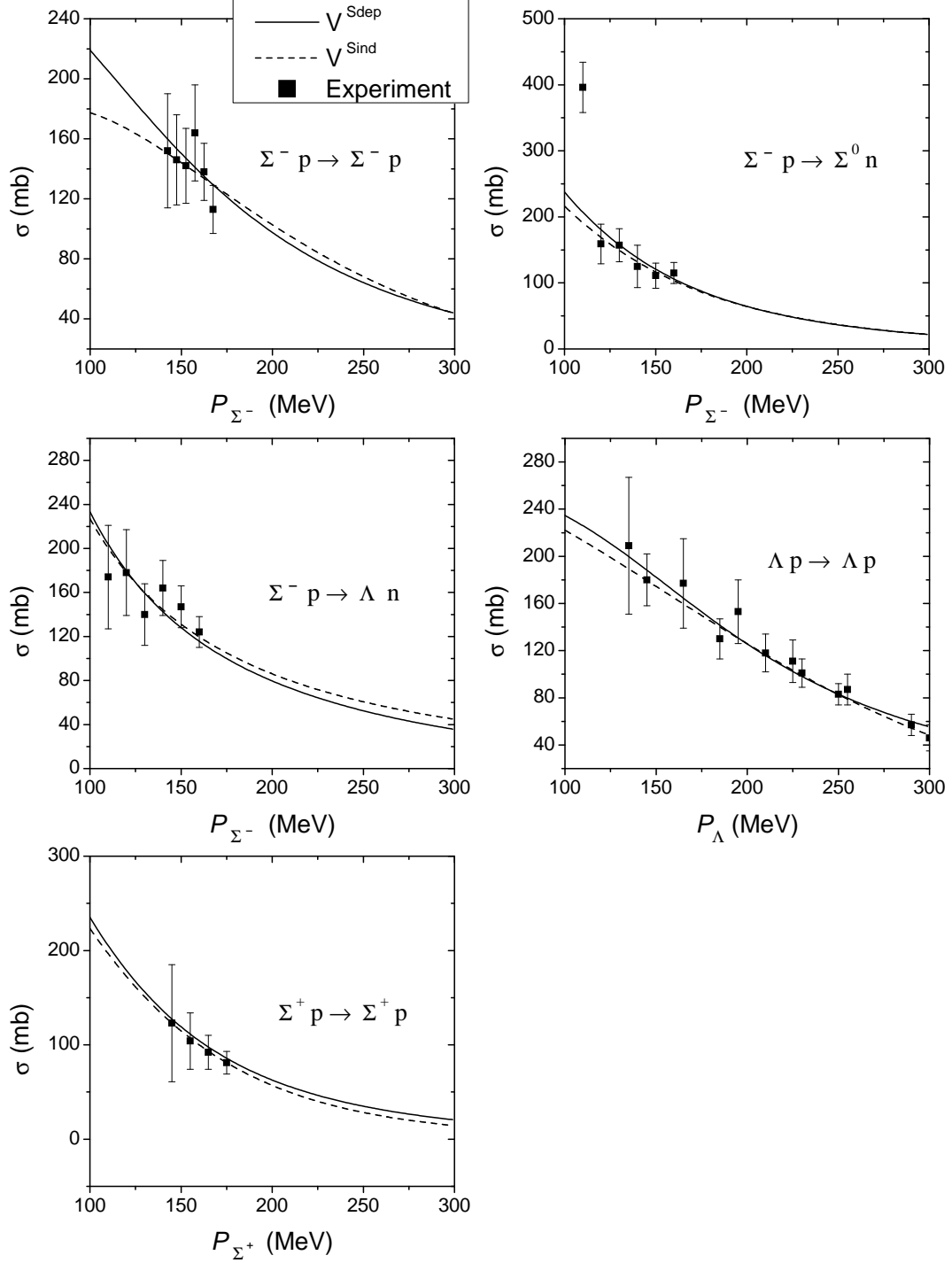


FIG. 9: Comparison of several theoretical cross-sections for the spin-dependent (solid line) and spin-independent (dashed line) coupled-channel $\Sigma N - \Lambda N$ potentials with experimental data [29–33] (data points).

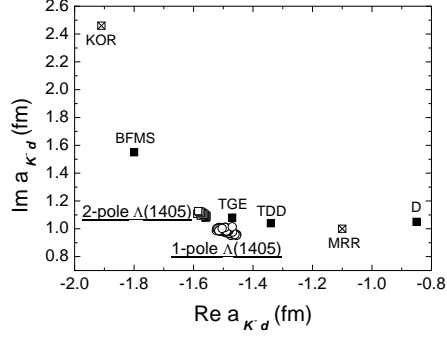


FIG. 10: The results of the full K^-d scattering length calculations using sets of one- (empty circles) and two-pole (empty squares) versions of $\bar{K}N - \pi\Sigma$ potential. Previous Faddeev calculations: BFMS [38], TGE [40], TDD [41], D [42] (filled squares), and FCA: KOR [34], MRR [39] (crossed squares) results are also shown.

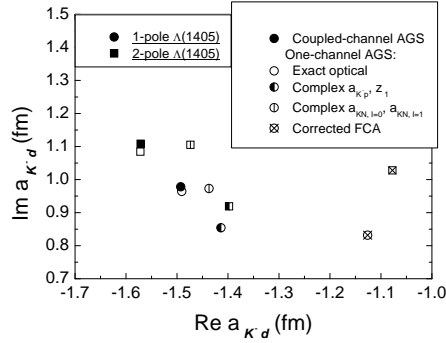


FIG. 11: Comparison of the full results of the a_{K^-d} calculations with representative one- (circles) and two-pole (squares) versions of $\bar{K}N - \pi\Sigma$ potential with approximate results. Values obtained with coupled-channel AGS equations (filled symbol), one-channel AGS with exact optical $\bar{K}N$ potential $V^{\bar{K}N}, \text{opt}$ (empty symbol), one-channel AGS with complex $V^{\bar{K}N}, \text{complex}_{(a,z)}$ (half-empty symbol) and $V^{\bar{K}N}, \text{complex}_{(a,a)}$ (vertically crossed symbol) results are shown. Results of corrected FCA formula using (crossed symbol) are also shown.

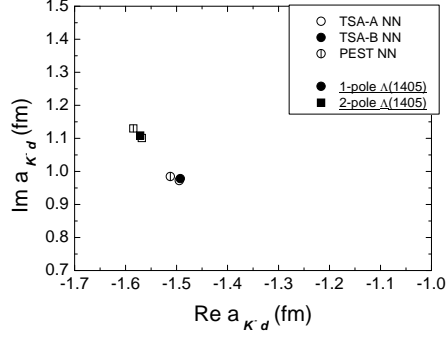


FIG. 12: Dependence of the full K^-d scattering length results on NN interaction: a_{K^-d} obtained with with TSA-A (empty symbol), TSA-B (filled symbol), and PEST (vertically crossed symbol) NN potentials. One- (circles) and two-pole (squares) representative versions of $\bar{K}N - \pi\Sigma$ interaction were used.

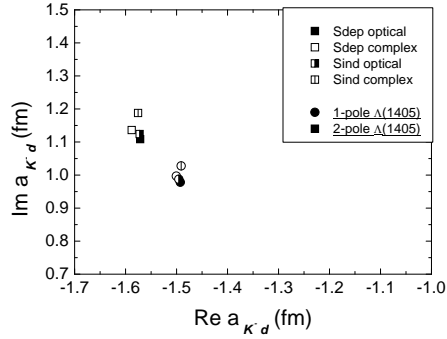


FIG. 13: Dependence of the full K^-d scattering length results on $\Sigma N - (\Lambda N)$ interaction. The a_{K^-d} values obtained with exact optical $V^{\text{Sdep,opt}}$ (filled square), simple complex $V^{\text{Sdep,complex}}$ (empty square), exact optical $V^{\text{Sind,opt}}$ (half-empty square), and simple complex $V^{\text{Sind,complex}}$ (vertically crossed square) are shown. One- (circles) and two-pole (squares) representative versions of $\bar{K}N - \pi\Sigma$ interaction were used.